Size-Dependent Subnanometer Pd Cluster (Pd_4, Pd_6, and Pd_{17}) Water Oxidation Electrocatalysis

Gihan Kwon,[†,#] Glen A. Ferguson,[†,#] Christopher J. Heard,[∥,#] Eric C. Tyo,[⊥] Chunrong Yin,[†] Janae DeBartolo,[‡] Sönke Seifert,[‡] Randall E. Winans,[‡] A. Jeremy Kropf,[§] Jeffrey Greeley,[∞] Roy L. Johnston,[∥] Larry A. Curtiss,[†,∞,*] Michael J. Pellin,[†,*] and Stefan Vajda[†,∞,⊥,*]

[†]Materials Science Division, [‡]X-ray Science Division, [§]Chemical Sciences and Engineering Division, and [∞]Nanoscience and Engineering Division, Argonne National Laboratory, 9700 South Cass Avenue, Argonne, Illinois 60439, United States, [∥]School of Chemistry, University of Birmingham, Edgbaston, Birmingham B15 2TT, United Kingdom, and [⊥]Department of Chemical and Environmental Engineering, School of Engineering & Applied Science, Yale University, 9 Hillhouse Avenue, New Haven, Connecticut 06520, United States. [#]These authors contributed equally to this work.

ABSTRACT Water oxidation is a key catalytic step for electrical fuel generation. Recently, significant progress has been made in synthesizing electrocatalytic materials with reduced overpotentials and increased turnover rates, both key parameters enabling commercial use in electrolysis or solar to fuels applications. The complexity of both the catalytic materials and the water oxidation reaction makes understanding the catalytic site critical to improving the process. Here we study water oxidation in alkaline conditions using size-selected clusters of Pd to probe the relationship between cluster size and the water oxidation reaction. We find that Pd_4 shows no reaction, while Pd_6 and Pd_{17} deposited clusters are among the most active (in terms of turnover rate per Pd atom) catalysts known. Theoretical calculations suggest that this striking difference may be a demonstration that bridging Pd−Pd sites (which are only present in three-dimensional clusters) are active for the oxygen evolution reaction in Pd_6O_6. The ability to experimentally synthesize size-specific clusters allows direct comparison to this theory. The support electrode for these investigations is ultrananocrystalline diamond (UNCD). This material is thin enough to be electrically conducting and is chemically/electrochemically very stable. Even under the harsh experimental conditions (basic, high potential) typically employed for water oxidation catalysts, UNCD demonstrates a very wide potential electrochemical working window and shows only minor evidence of reaction. The system (soft-landed Pd_4, Pd_6, or Pd_{17} clusters on a UNCD Si-coated electrode) shows stable electrochemical potentials over several cycles, and synchrotron studies of the electrodes show no evidence for evolution or dissolution of either the electrode material or the clusters.

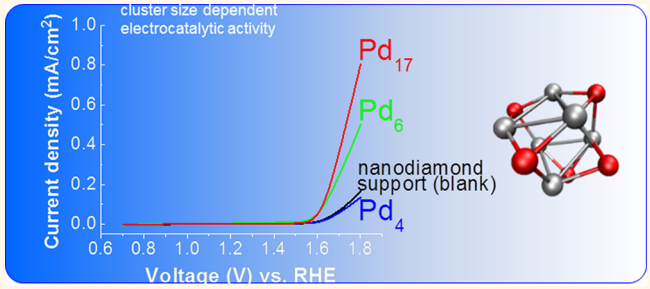

KEYWORDS: palladium · subnanometer clusters · nanocrystalline diamond · hybrid nanostructures · nanoparticles · catalysis · electrocatalysis · water oxidation · water splitting · X-ray absorption · GIXAS · GIXAFS · X-ray scattering · GISAXS

Efficient methods for splitting water are a key grand scientific challenge for meeting the world's fuel needs over the next century.[1−3] Electrochemical water splitting is a first step for the production of either H_2 or other fuels from the carbon oxides. It consists of two reactions—the hydrogen evolution reaction (HER) and the oxygen evolution reaction (OER). Of these, the OER is presently the least efficient, requiring a high overpotential (η = 0.3−0.5 V depending on the catalytic material and support chosen) for the reaction to proceed even at low turnover rates. The overpotential, η, is the potential required above the standard reaction potential (1.23 V at pH = 0). This critical step occurs in acid *via* the reaction $2H_2O \rightarrow 4H^+ + 4e^- + O_2$ and in base *via* the reaction $4OH^- \rightarrow 2H_2O + 4e^- + O_2$. In a fuel cell, where the inverse acid ORR is employed to produce energy, this poor catalytic performance results in the need for a high Pt catalyst loading on the cathode and adds significantly to the cost of this device.[4] In electrolyzers, the reaction in base is often employed to improve catalytic performance, and extensive recent effort has been employed to identify

* Address correspondence to vajda@anl.gov, pellin@anl.gov, curtiss@anl.gov.

Received for review February 14, 2013 and accepted June 25, 2013.

Published online June 25, 2013
10.1021/nn400772s

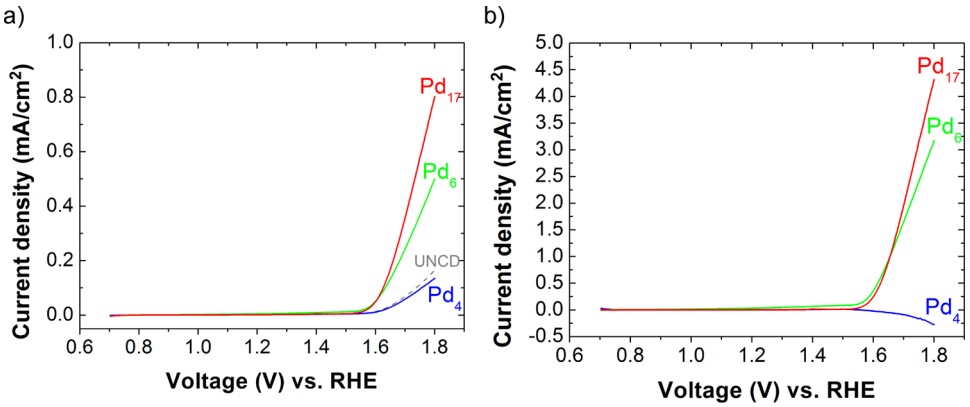

Figure 1. (a) Performance of size-selected palladium cluster on UNCD under pH 13.6 (1 M NaOH) with current densities normalized to the dipped chip area, S_{chip}, for the blank UNCD support (gray, dashed line), Pd_4 (blue), Pd_6 (green), and Pd_{17} (red) clusters. The fraction of surface area, $S_{cluster}$, covered by clusters was 9.4, 7.9, and 11.0% for the Pd_4, Pd_6, and Pd_{17} clusters, respectively, calculated as $S_{cluster}/S_{chip} \times 100$. (b) Background corrected (*i.e.*, after subtraction of the current of the blank UNCD support) currents normalized for the cluster-covered area.

more efficient, less expensive electrocatalysts for OER.[3,5−20]

Recently, we have had success in synthesizing subnanometer metal and metal oxide clusters with very narrow size distributions on thin film support materials (*e.g.*, alumina).[21−24] These materials show excellent activity and specificity for several heterogeneous, oxidative reactions[25−30] along with surprising stability.[23,24,31] Here we explore the efficiency and turnover rate for three Pd cluster sizes (Pd_4, Pd_6, and Pd_{17}) on thin ultrananocrystalline diamond (UNCD) supports for the OER. The study is important since (1) small clusters have not been explored for electrocatalysis, (2) clusters of this size are essentially single catalytic sites, (3) their activity can provide valuable insights into catalytic mechanisms, and (4) calculations can be done at sufficient accuracy to allow guidance for improvement.

We find that the system (soft-landed Pd_4, Pd_6, or Pd_{17} clusters on a UNCD-coated Si electrode) is stable under the harsh electrochemical conditions of the OER (pH = 13.1 at 1.8 V *vs* RHE). To our knowledge, this is the first demonstration that catalysts in this size range are stable as electrochemical electrodes. We also show that the overpotential and turnover frequency are strongly size-dependent. The best of these catalysts shows competitive efficiencies and very high turnover rates per atom (a unit of comparison that has been adopted by the thin film OER community[5,7,11,18]).

The dramatic cluster size dependence is particularly interesting given that our catalysts are deposited as essentially single catalytic sites and that our deposition method allows us to measure for the first time the number of "sites" on our electrodes. Density functional calculations were employed to explore the origin of the difference in electrochemical activity between the Pd_4 and Pd_x (x = 6 and 17) clusters. Calculations of the reaction thermodynamics under electrochemical conditions allow us to propose an explanation for the difference in reactivity based on cluster composition consistent with the experimental evidence.

RESULTS AND DISCUSSION

Oxygen Evolution Reaction Activity of Pd Subnanometer Clusters. The OER activity of three Pd clusters (Pd_4, Pd_6, and Pd_{17}) has been measured on an ultrananocrystalline diamond film electrode at pH 13.6 (1 M NaOH). Figure 1a shows linear sweep voltammetry (LSV) curves of Pd_4 (blue), Pd_6 (green), and Pd_{17} (red) clusters after 500 s cleaning by chronoamperometry at 1.7 V. A background curve (gray) for a UNCD-coated electrode without deposited Pd clusters is also shown. The blank UNCD used had the same dimensions and identical batch as the cluster-covered samples. Immediately apparent is the large increase in anodic current between Pd_6 (green) or Pd_{17} (red) and the UNCD support (gray). This difference is more remarkable considering that only about 10% of the total surface area of the electrode was coated with Pd clusters; moreover, within this area, as low as 0.1 atomic monolayer equivalent of Pd metal (1.5×10^{14} atoms/cm^2) was deposited.

In considering the cluster size dependence of OER activity, it is also clear that the activity of palladium clusters increases with particle size (see also Figure S1 in Supporting Information). A very interesting feature is observed for the smallest size Pd_4 clusters, where no increase in activity can be detected.

This is more apparent in Figure 1b, where background corrected (*i.e.*, after subtraction of the current of the blank UNCD support) currents normalized for the cluster-covered area. Here, a slight drop within the estimated uncertainty (see Methods section) is observed for Pd_4. We hypothesize that more careful studies might reveal that the drop is consistent with the fraction of UNCD surface sites blocked by the Pd_4 clusters, which may provide a selective route to "heal" surface defects where deterioration of the surface of the support may occur.

TABLE 1. Per Pd Cluster and Per Pd Atom Turnover Rates at 1.626 V *vs* RHE (η = 351 mV)[a]

cluster	TOR/Pd_n TOR per cluster (this work) [1 × $cluster^{-1}$ s^{-1}]	TOR/Pd TOR per total atom (this work) [1 × $atom^{-1}$ s^{-1}]	TOR/surface Pd atom (based on ref 7) (surface of bulk Pd) [1 × $atom^{-1}$ s^{-1}]	TOR/surface Co atom (based on ref 7) (CoOx on Au surface) [1 × $atom^{-1}$ s^{-1}]
Pd_4	−0.15	−0.038	0.024	1.24
Pd_6	4.03	0.68		
Pd_{17}	10.17	0.60		

[a] We note that water oxidation is a four-electron transfer process, so per electron rate has been divided by a factor of four. The turnover rates are compared to published studies of Pd metal and Co oxide deposited on Au.[7] In this table, we use the background corrected results displayed in Figure 1b. The reported values were calculated based on the background corrected current intensities plotted in Figure 1b and the knowledge of the metal loading of the immersed area. Based on the ∼5% estimated uncertainties in the metal loading, ∼10% estimated uncertainties in the determination of the immersed area and current measurement, the estimated uncertainty of the reported data is ∼15% or smaller.

Stability of the system is demonstrated in Figures S3 and S4. In Figure S3, we show that at an applied potential of 1.7 V *vs* RHE the current density shows an initial decay that stabilizes after a few minutes. We interpret this as an initial surface cleaning. Figure S4 demonstrates stable cyclic voltammetry data for the three cycles following the "cleaning" pulse. We note that this does not ensure "durability" for an extended period. However, their durability is sufficient to determine the catalytic properties of this catalytic site.

One unique aspect of the sample fabrication method here is the ability to use the deposition current to calculate accurately the number of deposited clusters (whose atom number represents an upper bound on the number of catalytic reaction sites). We have used the background corrected current of Figure 1b and the known concentration of deposited clusters to calculate the OER turnover rates. These data are displayed in Table 1.

Based on the ∼5% estimated uncertainties in the metal loading, ∼10% estimated uncertainties in the determination of the immersed area and current measurement, the estimated uncertainty of the reported data is better than 15%.

We have chosen to calculate these turnover rates at the same overpotential reported recently for water oxidation studies of several metal and cobalt oxide-coated metal electrodes at similar pH.[7]

Several interesting aspects are revealed by Table 1. First, as is clear in Figure 1, Pd_4 clusters supported on ultrananocrystalline diamond film electrodes if anything exhibit a small decrease in reactivity when compared to UNCD electrodes alone. A drop in activity might arise either from site blocking or from interactions that change the electronegativity of the UNCD surface atoms (such effects have been seen for the OER activity of Au clusters with small additions of Co[32]). The change points out a key assumption in calculating the per Pd atom and per Pd cluster turnover rates of these electrode materials, namely, that the support activity is not significantly changed by cluster deposition. The Pd_4 result supports this assumption. The turnover rates for Pd_6 and Pd_{17} are, in contrast to Pd_4, significant.

Table 1 compares the result of our cluster deposited electrodes to previous work on Pd metal and to ∼0.4 monolayers of cobalt oxide on Au.[7] Clearly these clusters are significantly more active than Pd metal surfaces. In fact, the activities are comparable to Ir (TOR = 0.64 $atom^{-1}$ s^{-1}),[7] the most active metal for OER, and to cobalt oxide deposited on Au electrodes (TOR = 1.24 $atom^{-1}$ s^{-1}).[7] It is also interesting to note that the per atom turnover rates of Pd_6 and Pd_{17} are similar despite the likelihood that only a fraction of the Pd_{17} atoms occupy surface sites, in contrast to Pd_6.

All cluster samples showed stable performance during four voltammetric cycles applied, with currents within the estimated experimental 5% uncertainty. Further, as explained below, the amount of Pd metal is also constant during cycling.

GIXAS Studies of Pd Cluster Electrodes. Following electrochemical cycling, the electrodes were investigated at the 10-ID beamline of Advanced Photon Source using grazing incidence X-ray absorption spectroscopy (GIXAS). Figure 2 displays GIXAS data, acquired for unimmersed (as deposited, black) and immersed, cycled (red) areas of electrodes with Pd_4 (Figure 2a,b), Pd_6 (Figure 2c,d), and Pd_{17} (Figure 2e,f) clusters investigated. The concordance of the XANES features of the bulk PdO standard and each cluster sample demonstrates that clusters' oxidation state resembles that of bulk PdO. The difference in the initial peak shape likely arises from subnanometer size effects, as also reported for other subnanometer size clusters.[36,42,43]

The purpose of this *ex situ* work was to compare the (re)oxidation properties of the three cluster sizes in a standard laboratory environment and to look for any potential lasting changes that might arise during electrochemical cycling. A comparison of the GIXAS spectra of Pd clusters with standards of Pd metal (gray, solid) and PdO (gray, dotted) reveal that all three cluster samples contain oxidized palladium species.

A comparison of immersed, cycled spectra with those that were never immersed indicates only very small changes resulting from electrochemical cycling under the conditions employed here (Figure 2a,c,e). The number of Pd atom absorbers in each sample is

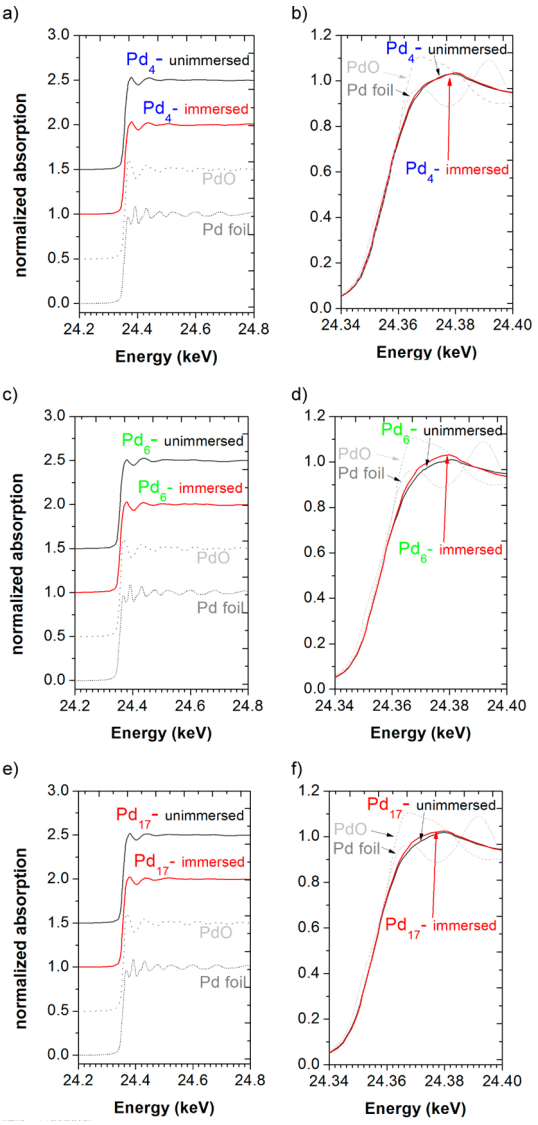

Figure 2. X-ray absorption spectra (left) and enlarged edge region (right) for unimmersed (as deposited, black) and immersed and cycled (red) areas of electrodes with Pd_4 (a,b), Pd_6 (c,d), and Pd_{17} (e,f) clusters investigated. An offset was applied on spectra for clarity in (a), (c), and (e). The spectra of bulk $Pd^{(0)}$ (foil) and $Pd^{(II)}O$ standards are shown, as well, for comparison.

within experimental error (~10%) identical. This demonstrates that Pd did not dissolve from our electrode during electrochemical experiments.

An expanded look at the near edge spectra (Figure 2b,d,f) indicates subtle differences for Pd_4 clusters in comparison with either Pd_6 or Pd_{17}. The almost identical spectra of immersed and unimmersed Pd_4 clusters (Figure 2b) indicate almost no difference in oxidation state caused by electrochemical cycling. Pd_6 and Pd_{17} clusters (Figure 2d,f) show a small oxidation state change. However, we note that these clusters as well remain clearly oxidized and that small changes such as these can arise during spectra processing. The most important finding from XAS is that the clusters remain largely unaffected, long-term, by electrochemical cycling. A change in the oxidizability as a function of cluster size may be a possible clue to significantly different catalytic activity of these clusters since several recent theoretical studies have commented on the sensitivity of the water oxidation reaction to the water absorption energy.[1,4,7,33] A much closer view of the role of the oxidation state of clusters will require *in situ* studies, however. In summary, for all clusters, GIXAS spectra obtained on the cycled and uncycled halves of the sample provide additional evidence of the stability and leach resistance of the subnanometer clusters (under harsh electrocatalytic conditions for the first time, to the best of our knowledge).

Grazing Incidence Small Angle X-ray Scattering (GISAXS) Studies of Pd Cluster Electrodes. We also collected GISAXS data on the samples following electrochemical cycling with the goal to investigate potential changes in cluster sizes and of the morphology of the thin support UNCD film. Figure 3 displays horizontal and vertical cuts of GISAXS data, acquired with photons of 24 keV energy, for unimmersed (as deposited, black) and immersed, cycled (red) areas of electrodes with Pd_4 (Figure 3a,b), Pd_6 (Figure 3c,d), and Pd_{17} (Figure 3e,f) clusters investigated, as well as a blank UNCD support (Figure 3g,h). The identical patterns of the scattering data obtained on the blank UNCD support indicate a stable support without a change in its morphology under electrocatalytic conditions (Figure 3g,h). Similarly, the identical, featureless GISAXS patterns for cluster electrodes (Figure 3a–f) show no evidence for the growth of nanometer-sized cluster aggregates. Previous studies demonstrate our ability to detect clusters above 1 nm with high sensitivity,[23,31,34,35] as well as earliest stage of agglomeration of subnanometer clusters.[30,36] It is worth emphasizing the lack of any feature of nanoparticle formation *via* aggregation of subnanometer clusters. This result coupled with GIXAS demonstration that Pd atoms are not lost confirms that our samples have sintering- and leaching-resistant subnanometer clusters under electrocatalytic conditions.

Density Functional Calculations of the O_2 Evolution Thermochemistry by Pd Subnanometer Clusters. An understanding of the palladium cluster OER can be gained by calculating the thermochemistry of the most important intermediates for each of the four-electron transfer electrochemical reactions required for water oxidation. The OER activity of each cluster type is investigated using the method of Rossmeisl *et al.*[3] In this method, the thermochemistry of each OER reaction step is calculated with respect to the reversible hydrogen electrode including the applied electrochemical potential. While this method has been previously used to model the water electrolysis on metal oxides surfaces (*e.g.*, RuO_2, IrO_2, and TiO_2),[3] to our knowledge, this is the first time it has been applied to subnanometer clusters.

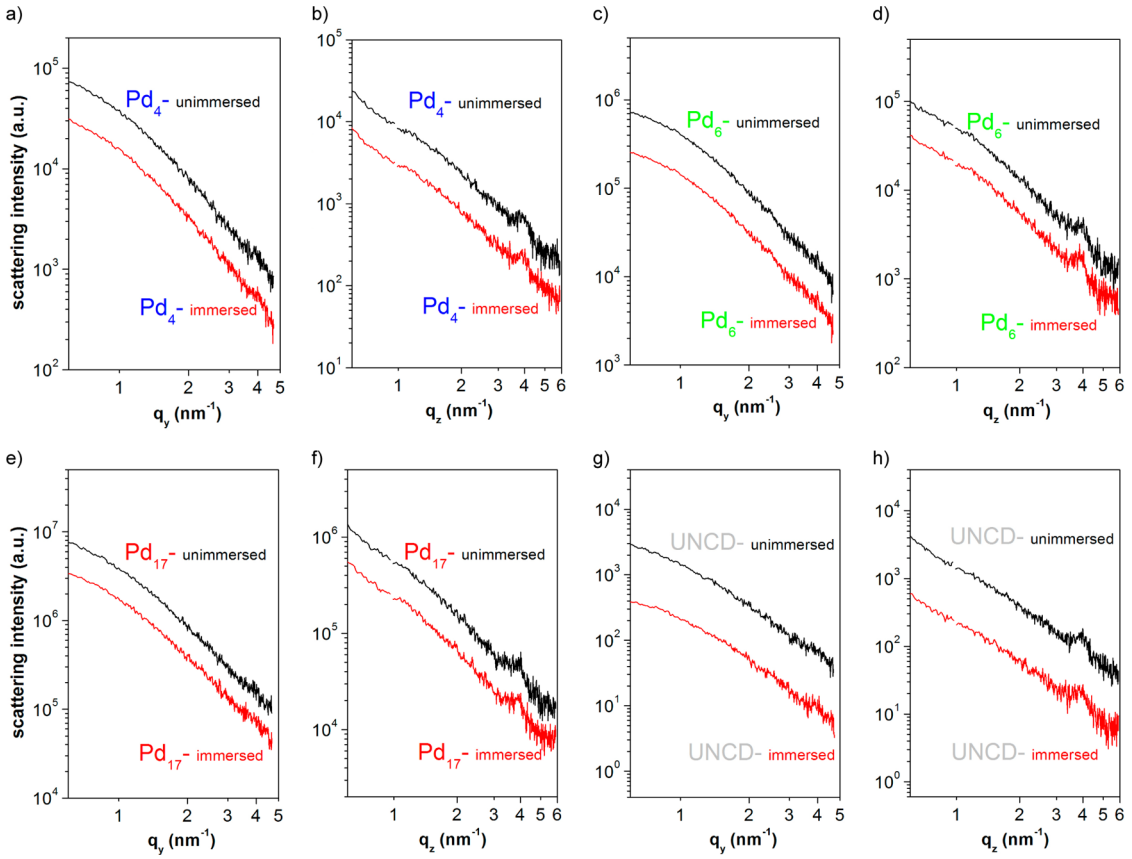

Figure 3. Horizontal (q_y) and vertical (q_z) cuts of the GISAXS data, acquired with photons of 24 keV energy, for unimmersed (as deposited) and immersed area for the Pd_4 (a,b), Pd_6 (c,d), and Pd_{17} (e,f) clusters investigated, as well as blank UNCD support (g, h). There was a similar offset applied for clarity between the unimmersed and immersed curves. The apparent peak at ~4 nm^{-1} in the vertical cuts is caused by scattering from the Kapton window; q_y and q_z denote scattering vectors in the horizontal and vertical plane, respectively.

The Rossmeisl *et al.*[3] method involves evaluating the thermodynamic potential required to drive each of the four-electron transfer reactions (Figure 4d) required for water oxidation. We note that this method should only be considered a first-order approximation due its neglect of kinetic barriers. In this method, the free energy change for each electron transfer step is calculated using the chemical potential of hydrogen, that is, $*AH \rightarrow *A + H^+ + e^-$ calculated as $*AH \rightarrow *A + 1/2H_2$.

An ideal catalyst would have a potential at each electron transfer step of 1.355 eV at a potential of 0 V on the reversible hydrogen scale (note that this is 1.23 V when referenced to the free energy of water), achieving the needed energy to drive the overall reaction at the lowest possible cell potential. Any thermodynamic step larger than this ideal minimum potential will result in an overpotential being needed to drive the OER reaction reducing the efficiency of the process. Any thermodynamic step smaller than this ideal potential results in the now necessary overpotential to be distributed among the remaining three reactions also lowering the OER efficiency.

Given the four-electron transfer reactions required, a physical realization of the ideal catalyst would have similar binding energy differences with respect to liquid water for each of the important reaction intermediates (O, OH, and OOH).

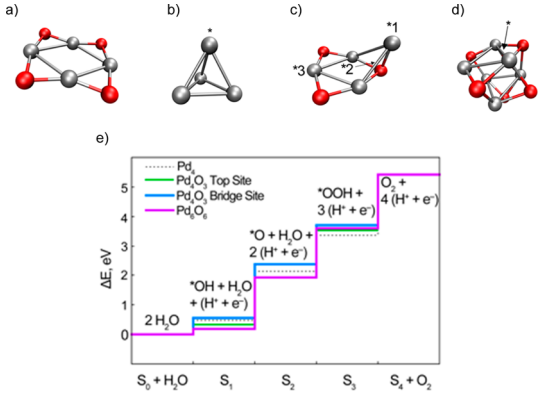

Figure 4. Structures used for calculation of the thermochemistry of the OER reactions ($S_0 \rightarrow S_4$ in e) of the (a) Pd_4O_4, (b) Pd_4, (c) Pd_4O_3, and (d) Pd_6O_6 clusters. For a–d, the "*" indicates the reaction sites. For the Pd_4O_3 cluster, three sites were explored labeled $*^1$ for site 1, $*^2$ for site 2, and $*^3$ for site 3. (e) Changes in free energy for the intermediates of the electrolysis of water by the subnanometer clusters: Pd_4 (dashed line), Pd_4O_3 site 1 (blue line), Pd_4O_3 site 2 (green line), and Pd_6O_6 (purple line) at U = 0 and pH = 0. The products and reactants for each of the four-electron transfer reactions are displayed on the $S_0 \rightarrow S_4$ steps. Here the "*" indicates a cluster attached product.

TABLE 2. ΔE and $\Delta\Delta E$ for Each Reaction Step of the Reactions Steps Shown in Figure 4e[a]

	OER palladium pathway							
	cluster							
	Pd_4		Pd_4O_3 top site		Pd_4O_3 bridge site		Pd_6O_6	
coordinate	ΔE	$\Delta\Delta E$	ΔE	$\Delta\Delta E$	ΔE	$\Delta\Delta E$	ΔE	$\Delta\Delta E$
$* + 2(H_2O)$	0.00		0.00		0.00		0.00	
$*OH + H_2O + (H^+ + e^-)$	0.47	0.47	0.31	0.31	0.55	0.55	0.19	0.19
$*O + H_2O + 2(H^+ + e^-)$	2.14	1.67	2.36	2.05	2.39	1.84	1.94	1.75
$*OOH + 3(H^+ + e^-)$	3.37	1.23	3.51	1.15	3.71	1.33	3.59	1.66
$* + 0_2 + 4(H^+ + e^-)$	5.42	2.06	5.42	1.92	5.42	1.71	5.42	1.83

[a] All values are in eV. The value of 0_2 is determined as a parameter of the equation $H_2O \rightarrow 1/2O_2 + 2H$ using the gas phase water values of ZPE = 0.56 eV and TS = 0.67 eV (0.035 bar and 300 K). The final value of the 0_2 energy is 9.55 eV. This avoids calculating the 0_2 energy which is poorly described by DFT.

The reactions for the chart in Figure 4e are as follows:

$$2H_2O \rightarrow *OH + (H^+ + e^-) \quad (1)$$

$$*OH + H_2O \rightarrow *O + 2(H^+ + e^-) \quad (2)$$

$$*O + H_2O \rightarrow *OOH + 3(H^+ + e^-) \quad (3)$$

$$*OOH \rightarrow O_2 + 4(H^+ + e^-) \quad (4)$$

Another mechanism is possible with the $*O + H_2O$ binding being replaced by 2 *OH binding; however, these calculations resulted in either an equal or higher overpotential for these clusters. Density functional calculations were used to determine the energy differences between the four reaction steps on a variety of gas phase Pd clusters chosen to help understand the experimental results. These clusters included Pd_4, Pd_4O_4, Pd_4O_3, and Pd_6O_6. The structures are given in Figure 4a–d. The Pd_4O_3, Pd_4O_4, and Pd_4 clusters used global minimum structures, while the Pd_6O_6 cluster is constructed by adding six oxygen atoms to the most stable bare metal cluster found in previous studies,[37] followed by complete geometric relaxation. The Supporting Information includes greater detail on structural optimization including information on Pd_4O_x (x = 0, 3, 4).

Among these clusters, the GIXAS studies described above and the strongly oxidizing conditions in the electrochemical cell at OER potentials suggest that the Pd_4O_4 and Pd_6O_6 clusters represent the oxidation states of the supported Pd_4 and Pd_6 clusters in the experiments. The Pd_4 cluster is included for reference. The key intermediates for the clusters in the OERs were calculated, and the resulting energies referenced to the RHE (Table 2 and Figure 4e).

For the Pd_6O_6 cluster, the only reaction site discovered that allows stable coordination of all three (O, OH, and OOH) species necessary for OER is labeled * and bridges two Pd atoms. For this site (as with all Pd clusters investigated), the largest energy difference occurs between the S_3 and S_4 reaction steps, which corresponds to the differences in the adsorption energies of the *OOH adsorbate and O_2 with respect to liquid water. This difference (U = 1.83 eV) corresponds to an overpotential of ~0.6 eV which is in reasonable agreement with experimental results shown above. These results are for gas phase Pd_6O_6. While calculations on supported Pd_x clusters are beyond the scope of this publication, the larger number of atoms in Pd_6O_6 and its three-dimensional nature provides reaction sites that are not proximate to the support.

For the Pd_4O_4 cluster, the only discovered reaction sites lead to unrealistically large geometric rearrangements upon O, OH, and OOH adsorption. This rearrangement is the result of a low Pd_4O_4 cluster atomization energy (0.9 eV/PdO unit less than Pd_6O_6). Therefore, the Pd_4O_4 results are not included in Figure 4e. Significant distortion is likely also to occur for a supported Pd_4O_4 cluster since all atoms are in contact with the surface due to the two-dimensional nature of the cluster (see Figure 4a). This theoretical result for the Pd_4O_4 cluster is consistent with the experimental studies above that show it is not active as an OER catalyst.

While Pd_4O_3 is unlikely to be present in the electrochemical cell at the potentials and pH needed to drive the OER, the Pd_4O_3 cluster structure allows theoretical investigation of the effects of local oxidation state and binding site geometry. We investigated four catalytic sites on the Pd_4O_3 cluster (two bridging, 2* and 4*, and two atop sites, 1* and 3*). Of these two sites, we find that only the 1*, 2*, and 3* sites in Figure 4c allow stable coordination of all three (O, OH, and OOH) species necessary for OER. We find a distinct difference in the catalytic efficiency of the bridging site when compared to either of the atop sites (1.84 eV at site 2* *vs* 2.05 eV at site 1* or 2.31 eV at site 3*). This is consistent with the results described above for Pd_6O_6 where the OER

reaction occurs on the bridging site. In both cases, this is due to a balanced O and OH adsorbate energy.

CONCLUSION

We have to our knowledge demonstrated for the first time that subnanometer clusters are stable enough electrocatalysts to allow their use for fundamental studies of catalytic processes. Further we have shown significant size dependence in their activity. We find that Pd_4 shows no reaction, while Pd_6 and Pd_{17} deposited clusters are among the most active (in terms of turnover rate per Pd atom) catalysts known.

Ex situ GIXAS studies and the strongly oxidizing conditions in the electrochemical cell at OER potentials suggest that the Pd_4O_4 and Pd_6O_6 clusters represent the oxidation states of the supported Pd_4 and Pd_6 clusters during OER and that the clusters are largely unaffected by electrochemical cycling. The ability to synthesize size-specific clusters with atomic precision allows direct comparison to this theory. Density functional calculations provide an explanation of the observed size dependence of the oxidized clusters.

Theoretical calculations suggest that this striking difference may be a demonstration that bridging Pd−Pd sites are active for the oxygen evolution reaction (OER) in Pd_6O_6. Overall, a key descriptor for an efficient OER Pd catalyst is a balancing of binding energy differences with respect to liquid water for each of the important reaction intermediates (O, OH, and OOH). This descriptor arises because the O, OH, and OOH binding energies govern the *E*'s of each of the four reaction steps. Thus at $U = 0$, optimization of this descriptor would result in the lowest overpotential. For these Pd clusters, the OOH is more strongly bound than the other species, resulting in the ~0.6 V overpotential observed.

In comparing the activity and efficiency of these subnanometer catalysts with the many catalysts that have been reported, it has been the most useful to review the work of Yao and Bell who have done a careful job of calculating turnover rates from the literature based on the number of surface atoms.[6,7]

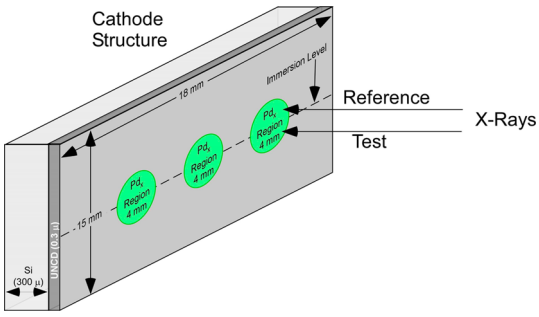

Figure 5. Schematics of the cluster-covered area on the sample immersed into the electrolyte showing three cluster spots of ~4 mm in diameter. The arrows below and above the central immersion line indicate the incident X-ray beams which, in addition to the determination of cluster area and position, were used to characterize by GISAXS and GIXANES the potential differences in particle size and oxidation state of the unimmersed (as deposited) and in electrolyte immersed exposed clusters, respectively.

The per atom turnover rates of these subnanometer Pd clusters are within a factor of 2 of the best reported values and are 100 times more active than a Pd metal electrodes (compared on a per surface atom basis under the conservative assumption that all cluster atoms participate in the reaction; see Supporting Information). As for efficiency, the overpotentials here are similar to those measured for the best catalysts—but not better.

Within these caveats, Pd clusters appear to be interesting and informative catalysts. In addition, it is likely that both the clusters and/or the support materials can be further optimized for the water oxidation reaction. For example, nanometer and larger Pd catalysts are not as active as Co or Ir catalysts. Further additions of other elements (*e.g.*, Ni) to Pd clusters has also been shown to significantly enhance activity.[14] Given that clusters in this size range are stable, we believe that the prospects for significant catalyst improvements are excellent. One approach to finding ideal clusters for water oxidation would be to carry out DFT studies of clusters to identify reaction descriptors and then screen for optimal clusters of different compositions and sizes.

METHODS

Figure 5 is a schematic of the cathodes used in this study. They consisted of a UNCD-coated Si wafer with three soft-landed (4 mm diameter) regions of clusters. A separate anode was prepared for each Pd cluster size (Pd_4, Pd_6, or Pd_{17}). Electrochemical studies were conducted with the cathode partially immersed in the electrolyte. This sample geometry was ideal for subsequent X-ray synchrotron studies of Pd cluster stability and oxidation state, allowing careful GISAXS and GIXAS of the potential differences in particle size and oxidation state of the unimmersed (as deposited) and in electrolyte immersed exposed clusters, respectively. The separate cluster deposition spots provided for an assessment of the uniformity of deposition. While advantageous for assessing the stability of clusters subjected to water oxidation (a primary purpose of this study), we recognize that is does raise some electrochemical issues. First, both Si and UNCD material (including their edges) are exposed during electrochemical cycling and in principle could contribute to the currents measured. Second, the presence of an air/liquid boundary can also lead to enhanced electrochemical current. We minimized the first issue by running identically prepared and processed Pd-free cathodes as a background test. These results demonstrate that the current produced is quite small when compared to signals from Pd catalyst electrodes. Subtraction of blank electrode currents then could be done without inducing significant additional errors. With these results, we minimized the second issue by rerunning OER reactions with the electrodes fully immersed (after synchrotron study). Here, enhanced currents were consistent with the added number of Pd clusters.

Support Material. Silicon wafers coated with a 0.3 μm thick ultrananocrystalline diamond film purchased from Advanced Diamond Technologies (UA25-100-0-p3)[38] were used as the support electrodes in this study. All electrodes used in this study were constructed from 15 × 18 mm size chips diced from the

same wafer. UNCD is an excellent support material for this study with a wide, flat potential window showing excellent stability under the harsh electrochemical oxidation conditions. The surface roughness of the wafers was ~7 nm rms, and the electrical conductivity of the B-doped silicon wafer/UNCD film combination of ~1 ohm·cm was sufficient to both allow controlled "soft-landing" of size-selected Pd clusters and to allow electrochemical studies. The wafers were used as purchased except for the dicing operation and for solvent cleaning prior to size-selected cluster deposition as described below.

Size-Selected Cluster Deposition. The size-selected subnanometer palladium cluster-based catalysts were prepared by depositing a narrow size distribution of palladium clusters generated in a laser vaporization cluster source. The size-selected cluster deposition method has been described in detail elsewhere.[25] In brief, a molecular beam of palladium clusters was generated by laser vaporization of a rotating palladium target using helium as a buffer gas. This continuous cluster beam was guided through ion optics and a quadrupole assembly. This assembly could be tuned to select clusters of a single nuclearity. Then mass-selected, positively charged clusters were directed onto the UNCD-coated Si wafer support. For the three cluster sizes chosen here (Pd_4, Pd_6, and Pd_{17}), the size distribution was 1, 2, and 3 atoms, respectively, around the main size (*i.e.*, 4 ± 1, 6 ± 2, and 17 ± 3 atoms per cluster). The kinetic energy of the clusters was controlled by electrical potentials placed on the wafer. This "soft-landing" method allowed deposition without subsequent agglomeration.

The amount of deposited palladium metal was determined by real-time monitoring of the deposition flux on the support. The total charge deposited could be determined with less than 5% uncertainty. In order to avoid possible aggregation of clusters on the surface, the surface coverage was chosen to be around 0.1 atomic ML equivalent of palladium metal for all samples, based on 1.53×10^{15} atoms/cm^2 of a Pd (111) plane. Three spots were deposited on each sample with size-selected clusters (see Figure 5). The exact position and diameter of the cluster-covered area was later determined by GIXAS at 12-ID-C beamline of the Advanced Photon Source, with an estimated uncertainty of 0.5 mm or better. The diameters of the cluster spots varied between 4 and 5 mm, depending on cluster size and deposition conditions.

Grazing Incidence Small-Angle X-ray Scattering. GISAXS was used to monitor possible changes in cluster size and in the morphology of the support material induced by the electrochemical environment by comparing the in electrolyte immersed and unimmersed parts of the cluster samples as well as the blank (*i.e.*, without clusters) UNCD support. GISAXS technique has proven to be very powerful for studying subnanometer and nanometer-sized particles at surfaces and their transformations under vacuum conditions as well as in a reactive gas environment.[34,35,39,40] Therefore, it can provide particle size distribution, distance between particles, and average aspect ratio of metal particles in reaction conditions. The GISAXS characterization was performed in helium environment using X-rays of 24.3 keV energy in a specially built reaction cell of unique design[26,28,29,36,41−44] at the 12-ID-C beamline of the Advanced Photon Source, by using a Mar 165 CCD (1024 × 1024 pixel) detector.

Grazing Incidence X-ray Absorption Spectroscopy (XAS). (X-ray absorption near-edge spectroscopy, XANES, and extended X-ray absorption fine structure spectroscopy, EXAFS) is a powerful technique that is able to monitor changes in oxidation state and local coordination environment of metal nanoparticles during the course of the catalytic reaction. Unlike the conventional approach, GIXAS provides information of near surface region especially when the incident beam is near to or below critical angle. Therefore, GIXAS shows enhanced surface sensitivity which allows monitoring chemical change in samples with fractional monolayer coverage. At the 10-ID beamline, GIXAS data were collected using a bent Laue crystal analyzer coupled to scintillation detectors. The analyzer was tuned to the Pd $K\alpha_1$ X-ray emission line.[45] The collected data were analyzed using the IFEFFIT interactive software package (with ATHENA and ARTEMIS graphical interfaces).[34,40,46] In addition to the characterization of the oxidation state of the clusters in the electrolyte immersed and unimmersed areas of the samples, GIXAS was also used for the determination of the exact area of the immersed cluster area by scanning the sample along the deposition spot (see Figure 5), at 12-ID-C by a 4-element Vortex fluorescence detector mounted parallel to the sample surface.

Electrochemical Measurements and Calculation of Turnover Rates. Electrochemical measurements of the samples were collected in a 3-arm van Dyne electrochemical cell housed in a home-built Faraday cage to minimize electrical noise and block stray room light during measurement. The compartment of working electrode has a flat quartz optical window (20 mm diameter) for photoelectrochemical measurements. Pt wire and Ag/AgCl (BASi Analytical Instruments, MR-5275) were used as the counter and reference electrodes, respectively. A Metrohm Autolab, μAUTOLAB III potentiostat with NOVA software was used to collect the electrochemical data, which were measured at room temperature. The electrolyte solution was 1 M NaOH (Fisher-Scientific, ACS grade), pH 14, prepared using Millipore water (Resistivity = 18.0 MΩ cm^{-1}, TOC < 5 ppb). For sample evaluation, only half of the area of the cluster spot was immersed into the electrolyte to measure the electrochemical current. Chronoamperometry (CA) was first performed with a potential of 0.7 mV *vs* Ag/AgCl to evaluate the stability of the catalyst under water oxidation conditions. Next, cyclic voltammetry (CV) was performed in the dark using a scan rate of 20 mV/s. Chronoamperometry was performed with an applied potential of 0.7 V *vs* Ag/AgCl for 500 s. Cyclic voltammetry measurements were recorded from −0.3 to 0.8 V *vs* Ag/AgCl—the starting potential was −0.3 V—with a scan rate of 20 mV/s.

The per Pd atom and per Pd_n cluster turnover rates (TOR) were determined using the current measured on the cluster samples after subtraction of the contribution by the blank UNCD support and the known number of deposited Pd atoms and clusters. Turnover rate (electron/cluster/s) was current density (mA/cm^2) from immersed cluster spot × immersed cluster spot area (cm^2) × number of atom per cluster × coulomb/s/number of atoms on 0.1 ML/elementary charge/1000. Based on the 5% or better estimated uncertainties in the metal loading, and 15% or better estimated uncertainties in the determination of the immersed area and current measurement, the estimated uncertainty of the reported TOR data is 15% or better.

Density Functional Calculations. Energies were calculated with Kohn−Sham density functional theory with a plane-wave basis set using the Vienna ab initio simulation package (VASP). The ion−electron interactions were described using the generalized gradient corrected PW91 functional and the PAW potentials with an energy cutoff of 400 eV. Calculations were spin-polarized. The species used a $20 \times 20 \times 20$ Å^3 supercell. The results were converged until the forces were 0.03 eV/Å. Rossmeisl *et al.*[3] previously described the method used to reference the free energies to those of the standard hydrogen electrode. Due to the poor description of the O−O bond in the O_2 molecule by standard GGA methods, the value for O_2 was calculated as a parameter in the free energy of the reaction $H_2O \rightarrow 1/2O_2 + H_2$ with the overall reaction energy set to the experimental value of 2.46 eV.

Birmingham Cluster Genetic Algorithm. The Birmingham cluster genetic algorithm (BCGA) is an unbiased global optimization method for gas phase clusters, containing a range of empirical potentials, including Murrell−Motram[47,48] and Gupta,[49−52] and this work employs the new DFT-GA mode.[53]

In general, an initial population of 10 clusters is randomly generated within a spherical simulation cell, set to be considerably larger than the diameter of the random cluster. This population of clusters is acted upon by mating and mutation operators and locally relaxed to form a set of progeny. Ranking according to a hyperbolic tangent fitness function allows for selection of the fittest elements to survive into a new generation, maintained at an approximately equal size to the previous one. The specific fitness functions, mutation, and mating operators are described in detail in refs 50 and 54. Cluster structures of Pd_4O_y, $x = 0$, 3, and 4, are globally optimized from

random initial geometries, using the BCGA calculated at the DFT level with a plane-wave pseudopotential approach within the Quantum Espresso[55] package. The Perdew–Berke–Ernzerhof hybrid exchange-correlation functional and ultrasoft pseudopotentials with nonlinear core corrections and a semicore d-orbital state for palladium atoms are employed for the calculation of electronic energies. Kinetic energy cutoffs are optimized and set to 40 Ry, along with a cutoff of 450 Ry for the calculation of charge density. Electronic states are considered to be converged if the change between successive scf steps is no greater than 1×10^{-7} Ry. The Methfessel–Paxton smearing scheme[56] is employed in order to improve efficiency of electronic convergence for metallic states. Local relaxation is performed by the Broyden–Fletcher–Goldfarb–Shanno scheme within Quantum Espresso, with total energy and total force convergence criteria of 1×10^{-4} Ry and 1×10^{-3} Ry a_0^{-1}, respectively.

Progeny are produced by means of mating through a mass-weighted version of the Deaven and Ho cut and splice procedure.[57] Mutation is a simple replacement by a new, randomly generated cluster, in order to maintain variation in the population, and is applied once for every 10 clusters. Convergence with respect to mutation and mating is deemed to have been obtained when the lowest energy cluster in a population changes by less than 1×10^{-2} Ry for five consecutive generations.

Conflict of Interest: The authors declare no competing financial interest.

Acknowledgment. Work was supported by the U.S. Department of Energy, BES Materials Sciences, under Contract DE-AC-02-06CH11357, with UChicago Argonne, LLC, operator of Argonne National Laboratory. The use of the Advanced Photon Source, an Office of Science User Facility operated for the U.S. Department of Energy (DOE) Office of Science by Argonne National Laboratory, was supported by the U.S. DOE under Contract No. DE-AC02-06CH11357. The authors acknowledge the use of Argonne Advanced Photon Source (the 12-ID-C and 10-ID beamlines) and S. Lee for his assistance at sample preparation, S. Riha and A. Martinson for the use and their advice at using their electrochemical testing setup, as well as N. Markovic for fruitful discussions. J.G. acknowledges support through a DOE Early Career Award. R.J. and C.H. acknowledge the University of Birmingham North America fund for travel to Argonne, and the Argonne's Center for Nanoscale Materials for computer resources.

Supporting Information Available: Additional GIXANES, chronoampermetry and cyclic voltammetry data plots, and results of DFT calculations on Pd_4 and Pd_4O_y (y = 3,4) clusters. This material is available free of charge *via* the Internet at http://pubs.acs.org.

REFERENCES AND NOTES

1. Suntivich, J.; May, K. J.; Gasteiger, H. A.; Goodenough, J. B.; Shao-Horn, Y. A Perovskite Oxide Optimized for Oxygen Evolution Catalysis from Molecular Orbital Principles. *Science* **2011**, *334*, 1383–1385.
2. Vojvodic, A.; Norskov, J. K. Optimizing Perovskites for the Water-Splitting Reaction. *Science* **2011**, *334*, 1355–1356.
3. Rossmeisl, J.; Qu, Z. W.; Zhu, H.; Kroes, G. J.; Norskov, J. K. Electrolysis of Water on Oxide Surfaces. *J. Electroanal. Chem.* **2007**, *607*, 83–89.
4. Stephens, I. E. L.; Bondarenko, A. S.; Gronbjerg, U.; Rossmeisl, J.; Chorkendorff, I. Understanding the Electrocatalysis of Oxygen Reduction on Platinum and Its Alloys. *Energy Environ. Sci.* **2012**, *5*, 6744–6762.
5. Jiao, F.; Frei, H. Nanostructured Cobalt and Manganese Oxide Clusters as Efficient Water Oxidation Catalysts. *Energy Environ. Sci.* **2010**, *3*, 1018–1027.
6. Yeo, B. S.; Bell, A. T. *In Situ* Raman Study of Nickel Oxide and Gold-Supported Nickel Oxide Catalysts for the Electrochemical Evolution of Oxygen. *J. Phys. Chem. C* **2012**, *116*, 8394–8400.
7. Yeo, B. S.; Bell, A. T. Enhanced Activity of Gold-Supported Cobalt Oxide for the Electrochemical Evolution of Oxygen. *J. Am. Chem. Soc.* **2011**, *133*, 5587–5593.
8. Perez-Alonso, F. J.; McCarthy, D. N.; Nierhoff, A.; Hernandez-Fernandez, P.; Strebel, C.; Stephens, I. E. L.; Nielsen, J. H.; Chorkendorff, I. The Effect of Size on the Oxygen Electroreduction Activity of Mass-Selected Platinum Nanoparticles. *Angew. Chem., Int. Ed.* **2012**, *51*, 4641–4643.
9. Man, I. C.; Su, H. Y.; Calle-Vallejo, F.; Hansen, H. A.; Martinez, J. I.; Inoglu, N. G.; Kitchin, J.; Jaramillo, T. F.; Norskov, J. K.; Rossmeisl, J. Universality in Oxygen Evolution Electrocatalysis on Oxide Surfaces. *ChemCatChem* **2011**, *3*, 1159–1165.
10. Lin, Y. J.; Zhou, S.; Sheehan, S. W.; Wang, D. W. Nanonet-Based Hematite Heteronanostructures for Efficient Solar Water Splitting. *J. Am. Chem. Soc.* **2011**, *133*, 2398–2401.
11. Chou, N. H.; Ross, P. N.; Bell, A. T.; Tilley, T. D. Comparison of Cobalt-Based Nanoparticles as Electrocatalysts for Water Oxidation. *ChemSusChem* **2011**, *4*, 1566–1569.
12. Blakemore, J. D.; Schley, N. D.; Olack, G. W.; Incarvito, C. D.; Brudvig, G. W.; Crabtree, R. H. Anodic Deposition of a Robust Iridium-Based Water-Oxidation Catalyst from Organometallic Precursors. *Chem. Sci.* **2011**, *2*, 94–98.
13. Watt, J.; Cheong, S.; Toney, M. F.; Ingham, B.; Cookson, J.; Bishop, P. T.; Tilley, R. D. Ultrafast Growth of Highly Branched Palladium Nanostructures for Catalysis. *ACS Nano* **2010**, *4*, 396–402.
14. Singh, J. P.; Zhang, X. G.; Li, H. L.; Singh, A.; Singh, R. N. Electrocatalytic Activities of Pd–Ni Nanoparticles Obtained on Multiwalled Carbon Nanotubes towards Oxygen Evolution in 1M KOH. *Int. J. Electrochem.* **2008**, *3*, 416–426.
15. Lyons, M. E. G.; Brandon, M. P. The Oxygen Evolution Reaction on Passive Oxide Covered Transition Metal Electrodes in Alkaline Solution. Part III - Iron. *Int. J. Electrochem.* **2008**, *3*, 1463–1503.
16. Kanan, M. W.; Nocera, D. G. *In Situ* Formation of an Oxygen-Evolving Catalyst in Neutral Water Containing Phosphate and Co^{2+}. *Science* **2008**, *321*, 1072–1075.
17. Nakagawa, T.; Bjorge, N. S.; Murray, R. W. Electrogenerated IrO_x Nanoparticles as Dissolved Redox Catalysts for Water Oxidation. *J. Am. Chem. Soc.* **2009**, *131*, 15578–15579.
18. Esswein, A. J.; McMurdo, M. J.; Ross, P. N.; Bell, A. T.; Tilley, T. D. Size-Dependent Activity of Co_3O_4 Nanoparticle Anodes for Alkaline Water Electrolysis. *J. Phys. Chem. C* **2009**, *113*, 15068–15072.
19. Subbaraman, R.; Tripkovic, D.; Chang, K. C.; Strmcnik, D.; Paulikas, A. P.; Hirunsit, P.; Chan, M.; Greeley, J.; Stamenkovic, V.; Markovic, N. M. Trends in Activity for the Water Electrolyser Reactions on 3d M(Ni,Co,Fe,Mn) Hydr(oxy)oxide Catalysts. *Nat. Mater.* **2012**, *11*, 550–557.
20. Wang, C.; Markovic, N. M.; Stamenkovic, V. R. Advanced Platinum Alloy Electrocatalysts for the Oxygen Reduction Reaction. *ACS Catal.* **2012**, *2*, 891–898.
21. Deng, W.; Lee, S.; Libera, J. A.; Elam, J. W.; Vajda, S.; Marshall, C. L. Cleavage of the C–O–C Bond on Size-Selected Subnanometer Cobalt Catalysts and on ALD-Cobalt Coated Nanoporous Membranes. *Appl. Catal., A* **2011**, *393*, 29–35.
22. Vajda, S.; Lee, S.; Sell, K.; Barke, I.; Kleibert, A.; von Oeynhausen, V.; Meiwes-Broer, K.-H.; Rodriguez, A. F.; Elam, J. W.; Pellin, M. M.; *et al.* Combined Temperature-Programmed Reaction and *In Situ* X-ray Scattering Studies of Size-Selected Silver Clusters under Realistic Reaction Conditions in the Epoxidation of Propene. *J. Chem. Phys.* **2009**, *131*, 121104.
23. Vajda, S.; Winans, R. E.; Elam, J. W.; Lee, B.; Pellin, M. J.; Seifert, S.; Tikhonov, G. Y.; Tomczyk, N. A. Supported Gold Clusters and Cluster-Based Nanomaterials: Characterization, Stability and Growth Studies by *In Situ* GISAXS under Vacuum Conditions and in the Presence of Hydrogen. *Top. Catal.* **2006**, *39*, 161–166.
24. Winans, R. E.; Lee, B.; Seifert, S.; Lee, S.; Elam, J. W.; Pellin, M. J.; Barke, I.; Kleiber, A.; Sell, K.; von Oeynhause, V.; *et al.* Grazing Incidence Small-Angle X-ray Scattering Studies of Nano-Metal Catalysts. *Prepr. Pap. – Am. Chem. Soc., Div. Fuel Chem.* **2009**, *54*, 114–115.
25. Winans, R. E.; Vajda, S.; Ballentine, G. E.; Elam, J. W.; Lee, B.; Pellin, M. J.; Seifert, S.; Tikhonov, G. Y.; Tomczyk, N. A. Reactivity of Supported Platinum Nanoclusters Studied by

In Situ GISAXS: Clusters Stability under Hydrogen. *Top. Catal.* **2006**, *39*, 145–149.
26. Lee, S.; Molina, L. M.; Lopez, M.; Alonso, J. A.; Hammer, B.; Lee, B.; Seifert, S.; Winans, R. E.; Elam, J. W.; Pellin, M. J.; *et al.* Selective Propene Epoxidation on Immobilized Au_{6-10} Clusters: The Effect of Hydrogen and Water on Activity and Selectivity. *Angew. Chem., Int. Ed.* **2009**, *48*, 1467–1471.
27. Vajda, S.; Pellin, M. J.; Greeley, J. P.; Marshall, C. L.; Curtiss, L. A.; Ballentine, G. A.; Elam, J. W.; Catillon-Mucherie, S.; Redfern, P. C.; Mehmood, F.; *et al.* Subnanometre Platinum Clusters as Highly Active and Selective Catalysts for the Oxidative Dehydrogenation of Propane. *Nat. Mater.* **2009**, *8*, 213–216.
28. Lei, Y.; Mehmood, F.; Lee, S.; Greeley, J.; Lee, B.; Seifert, S.; Winans, R. E.; Elam, J. W.; Meyer, R. J.; Redfern, P. C.; *et al.* Increased Silver Activity for Direct Propylene Epoxidation *via* Subnanometer Size Effects. *Science* **2010**, *328*, 224–228.
29. Molina, L. M.; Lee, S.; Sell, K.; Barcaro, G.; Fortunelli, A.; Lee, B.; Seifert, S.; Winans, R. E.; Elam, J. W.; Pellin, M. J.; *et al.* Size-Dependent Selectivity and Activity of Silver Nanoclusters in the Partial Oxidation of Propylene to Propylene Oxide and Acrolein: A Joint Experimental and Theoretical Study. *Catal. Today* **2011**, *160*, 116–130.
30. Lee, S.; Lee, B.; Mehmood, F.; Seifert, S.; Libera, J. A.; Elam, J. W.; Greeley, J.; Zapol, P.; Curtiss, L. A.; Pellin, M. J.; *et al.* Oxidative Decomposition of Methanol on Subnanometer Palladium Clusters: The Effect of Catalyst Size and Support Composition. *J. Phys. Chem. C* **2010**, *114*, 10342–10348.
31. Vajda, S.; Winans, R. E.; Elam, J. W.; Lee, B.; Pellin, M. J.; Riley, S. J.; Seifert, S.; Tikhonov, G. Y.; Tomczyk, N. A. *In Situ* GISAXS Studies of the Thermal Stability and Temperature Induced Growth of Supported Cluster-Based Platinum and Gold Nanoparticles. *Prepr. Pap. – Am. Chem. Soc., Div. Fuel Chem.* **2005**, *50*, 190–191.
32. Hongfei, L.; Wei, T.; Kleiman-Shwarsctein, A.; McFarland, E. W. Oxygen Electroreduction on Gold–Cobalt Oxide Binary Nanocluster Catalysts. *J. Electrochem. Soc.* **2008**, *155*, B200-6.
33. Ferguson, G. A.; Mehmood, F.; Rankin, R. B.; Greeley, J. P.; Vajda, S.; Curtiss, L. A. Exploring Computational Design of Size-Specific Subnanometer Clusters Catalysts. *Top. Catal.* **2012**, *55*, 353–365.
34. Lee, B.; Seifert, S.; Riley, S. J.; Tikhonov, G.; Tomczyk, N. A.; Vajda, S.; Winans, R. E. Anomalous Grazing Incidence Small-Angle X-ray Scattering Studies of Platinum Nanoparticles Formed by Cluster Deposition. *J. Chem. Phys.* **2005**, *123*, 074701.
35. Winans, R. E.; Vajda, S.; Lee, B.; Riley, S. J.; Seifert, S.; Tikhonov, G. Y.; Tomczyk, N. A. Thermal Stability of Supported Platinum Clusters Studied by *In Situ* GISAXS. *J. Phys. Chem. B* **2004**, *108*, 18105–18107.
36. Lee, S.; DiVece, M.; Lee, B.; Seifert, S.; Winans, R. E.; Vajda, S. Support-Dependent Performance of Size-Selected Subnanometer Cobalt Cluster-Based Catalysts in the Dehydrogenation of Cyclohexene. *ChemCatChem* **2012**, *4*, 1632–1637.
37. vanSanten, R. A. The Cluster Approach to Molecular Heterogeneous Catalysis. *J. Mol. Catal., A* **1997**, *115*, 405–419.
38. Advanced Diamond Technologies, Inc. http://www.thindiamond.com/ (accessed August 6, 2012).
39. Yavuz, C. T.; Lee, S.; Lee, B.; Kim, M. H.; Baik, J. M.; Seifert, S.; Vajda, S.; Larson, C.; Winans, R. E.; Moskovits, M.; *et al. In Situ* Real Time Monitoring of Pt-VO_2 Nanoparticle-Nanowire Assembly by GISAXS. In *Micro- and Nanotechnology Sensors, Systems, and Applications II*; George, T., Islam, M. S., Dutta, A. K., Eds.; SPIE: Bellingham, WA, 2010; Vol. 7679, pp 76792D1–76792D9.
40. Wyrzgol, S. A.; Schafer, S.; Lee, S.; Lee, B.; Di Vece, M.; Li, X. B.; Seifert, S.; Winans, R. E.; Stutzmann, M.; Lercher, J. A.; *et al.* Combined TPRx, *In Situ* GISAXS and GIXAS Studies of Model Semiconductor-Supported Platinum Catalysts in the Hydrogenation of Ethene. *Phys. Chem. Chem. Phys.* **2010**, *12*, 5585–5595.
41. Lee, S.; Lee, B.; Seifert, S.; Vajda, S.; Winans, R. E. Simultaneous Measurement of X-ray Small Angle Scattering, Absorption and Reactivity: A Continuous Flow Catalysis Reactor. *Nucl. Instrum. Methods Phys. Res., Sect. A* **2011**, *649*, 200–203.
42. Ferguson, G. A.; Yin, C.; Kwon, G.; Tyo, E. C.; Lee, S.; Greeley, J. P.; Zapol, P.; Lee, B.; Seifert, S.; Winans, R. E.; *et al.* Stable Subnanometer Cobalt Oxide Clusters on Ultrananocrystalline Diamond and Alumina Supports: Oxidation State and the Origin of Sintering Resistance. *J. Phys. Chem. C* **2012**, *116*, 24027–24034.
43. Lee, S.; Vece, M. D.; Lee, B.; Seifert, S.; Winans, R. E.; Vajda, S. Oxidative Dehydrogenation of Cyclohexene on Size Selected Subnanometer Cobalt Clusters: Improved Catalytic Performance *via* Evolution of Cluster-Assembled Nanostructures. *Phys. Chem. Chem. Phys.* **2012**, *14*, 9336–9342.
44. Tyo, E. C.; Yin, C.; Di Vece, M.; Qian, Q.; Kwon, G.; Lee, S.; Lee, B.; DeBartolo, J. E.; Seifert, S.; Winans, R. E.; *et al.* Oxidative Dehydrogenation of Cyclohexane on Cobalt Oxide (Co_3O_4) Nanoparticles: The Effect of Particle Size on Activity and Selectivity. *ACS Catal.* **2012**, *2*, 2409–2423.
45. Kropf, A. J.; Finch, R. J.; Fortner, J. A.; Aase, S.; Karanfil, C.; Segre, C. U.; Terry, J.; Bunker, G.; Chapman, L. D. Bent Silicon Crystal in the Laue Geometry To Resolve X-ray Fluorescence for X-ray Absorption Spectroscopy. *Rev. Sci. Instrum.* **2003**, *74*, 4696–4702.
46. Ravel, B.; Newville, M. Athena, Artemis, HephaestusS: Data Analysis for X-ray Absorption Spectroscopy Using IFEFFIT. *J. Synchrotron Radiat.* **2005**, *12*, 537–541.
47. Murrell, J. N.; Mottram, R. E. Potential Energy Functions for Atomic Solids. *Mol. Phys.* **1990**, *69*, 571–585.
48. Lloyd, L. D.; Johnston, R. L.; Roberts, C.; Mortimer-Jones, T. V. Geometry Optimisation of Aluminium Clusters Using a Genetic Algorithm. *ChemPhysChem* **2002**, *3*, 408–415.
49. Cleri, F.; Rosato, V. Tight-Binding Potentials for Transition Metals and Alloys. *Phys. Rev. B* **1993**, *48*, 22–33.
50. Massen, C.; Mortimer-Jones, T. V.; Johnston, R. L. Geometries and Segregation Properties of Platinum-Palladium Nanoalloy Clusters. *J. Chem. Soc., Dalton Trans.* **2002**, 4375–4388.
51. Nunez, S.; Johnston, R. L. Structures and Chemical Ordering of Small Cu–Ag Clusters. *J. Phys. Chem. C* **2010**, *114*, 13255–13266.
52. Wilson, N. T.; Johnston, R. L. A Theoretical Study of Atom Ordering in Copper–Gold Nanoalloy Clusters. *J. Mater. Chem.* **2002**, *12*, 2913–2922.
53. Heiles, S.; Logsdail, A. J.; Schaefer, R.; Johnston, R. L. Dopant-Induced 2D–3D Transition in Small Au-Containing Clusters: DFT-Global Optimisation of 8-Atom Au–Ag Nanoalloys. *Nanoscale* **2012**, *4*, 1109–1115.
54. Rapallo, A.; Rossi, G.; Ferrando, R.; Fortunelli, A.; Curley, B. C.; Lloyd, L. D.; Tarbuck, G. M.; Johnston, R. L. Global Optimization of Bimetallic Cluster Structures. I. Size-Mismatched Ag–Cu, Ag–Ni, and Au–Cu Systems. *J. Chem. Phys.* **2005**, *122*, 194308.
55. Giannozzi, P.; Baroni, S.; Bonini, N.; Calandra, M.; Car, R.; Cavazzoni, C.; Ceresoli, D.; Chiarotti, G. L.; Cococcioni, M.; Dabo, I.; *et al.* Quantum Espresso: A Modular and Open-Source Software Project for Quantum Simulations of Materials. *J. Phys.: Condens. Matter* **2009**, *21*, 395502.
56. Methfessel, M.; Paxton, A. T. High-Precision Sampling for Brillouin-Zone Integration in Metals. *Phys. Rev. B* **1989**, *40*, 3616–3621.
57. Deaven, D. M.; Ho, K. M. Molecular-Geometry Optimization with a Genetic Algorithm. *Phys. Rev. Lett.* **1995**, *75*, 288–291.